(Received 14 August 2024, Accepted 22 October 2024, Scheduled 11 January 2025)

An Interleaved Dual-Band Outline Elliptical Dipole Antenna

Jonathan Marquardt[1], Maria Pour[1,*], and Curtis Hill[2]

[1]*Department of Electrical and Computer Engineering, The University of Alabama in Huntsville, Huntsville, AL 35899, USA*
[2]*NASA Marshall Space Flight Center, ESSCA, Huntsville, AL 35808, USA*

ABSTRACT: A new dual-band antenna is presented for the use in space-based passive energy harvesting. This antenna is based on elliptical dipole antennas, whose inner metallization is removed, leaving an outline antenna and room for a second set of antenna arms. This will in turn result in an interleaved structure to tune each set of dipole arms to two different frequencies. Due to the close proximity of the dipole arms, there exists strong mutual coupling, which is lessened by adding decoupling elements to the design. The proposed antenna is supported by a partial ground plane to improve the front-to-back ratio of the radiation patterns. The ground plane is extended with an exponential taper, and additional parasitic elements are added to improve antenna performance. The dual-band elliptical outline design was fabricated and measured, and the results are found in good agreement with simulation. This antenna design provides 14 dB return loss, 3.4 dBi peak gain, and 12 dB front-to-back ratio for both the 0.915 GHz and 2.45 GHz bands, making it a useful antenna for applications such as passive energy harvesting that require lightweight dual-band designs.

1. INTRODUCTION

For many antenna applications, size, weight, cost, and complexity are crucial considerations. A low-profile dual-band antenna is thus desired for a NASA application in space-based passive energy harvesting. This antenna operates in the 0.915 GHz and 2.45 GHz bands, and is desired to have at least 10 dB return loss, 10 dB front-to-back ratio, and positive peak gain in the forward direction, preferably greater than 3 dBi. An omnidirectional radiation pattern as seen in a dipole would be valuable to increase the received power as well [1]. As such, a double-sided printed dipole type antenna was chosen due to its low-cost, low-profile, and wideband properties [2]. If additional bandwidth is desired, each arm of the dipole element can be replaced with an elliptical patch [3].

In both the elliptical dipoles and the related wideband bowtie design, the literature suggests that it is not necessary to fill the full area occupied by the dipole arms with a conductor to achieve good impedance matching and efficient radiation since the surface current density is mainly concentrated at the edges [4–7]. At eccentricities close to zero (nearly circular), these elliptical loops behave like circular loop antennas, but at higher eccentricities the elliptical loops behave more similarly to dipoles [8]. Planar elliptical dipoles with elliptical slots have been studied for ultra-wideband applications and found to have increased gain and impedance bandwidth [9–11]. Many low-profile, compact designs for dual-band and multi-band antennas have been proposed [12–15]. Some multi-band antennas have been studied in which the inner metallization of an antenna element is removed and the resulting empty space filled with additional, smaller elements. These smaller elements are tuned to radiate at the higher frequencies of interest [16, 17].

In this article, a dual-band outline elliptical dipole antenna is proposed. Starting with a double-sided printed elliptical dipole, the interior metallization is removed. This has minimal effects on the radiation characteristics in the band of interest while creating space for upper-band elements, which are placed on the opposite side of the board to their lower-band counterparts. Finally, parasitic and reflective elements are inserted into the design to reduce mutual coupling and allow for independent tuning of each band. A prototype of this antenna was measured, achieving at least 14 dB return loss, 3.4 dBi peak gain, and 12 dB front-to-back ratio in each band, making it an excellent candidate for space-based passive energy harvesting applications.

2. DUAL-BAND ELLIPTICAL ANTENNA DESIGN

Figure 1 shows the geometry of the proposed antenna. Its overall dimensions ($B \times B$) are $150 \times 150\,\text{mm}^2$, and the substrate is 0.11 mm thick Rogers Kappa 438 ($\varepsilon_r = 4.38$). To achieve dual-band operation, this antenna consists of two sets of outline elliptical antenna arms. The upper-band arms are nested within the lower-band arms and mirrored to the opposite side of the board. To improve the front-to-back ratio, the ground plane was given an exponential taper at the sides, and reflective elements were added behind the upper-band elements. Finally, due to the strong electromagnetic coupling between these closely-spaced arms, parasitic decoupling strips were added to help improve the impedance matching.

To demonstrate the importance of the additional reflecting and parasitic elements, the S_{11} and radiation characteristics are therefore presented in Figs. 2 and 3, respectively, by comparing the antennas without these elements, with just one of these features, and finally an antenna with both additional elements.

* Corresponding author: Maria Pour (maria.pour@uah.edu).

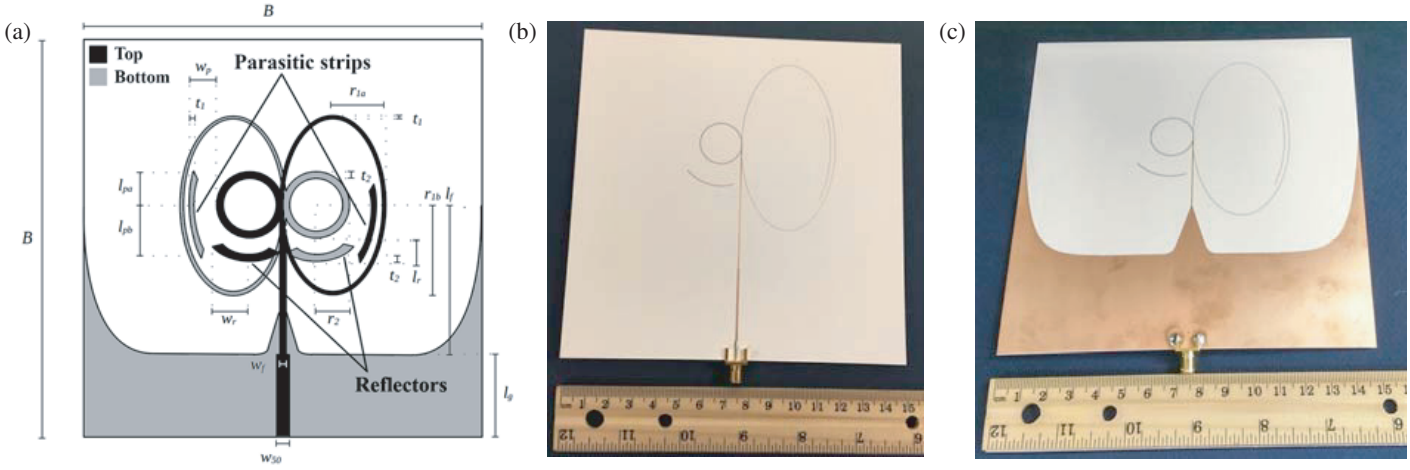

FIGURE 1. (a) Geometry, (b) top-side of prototype, and (c) bottom-side view of the proposed antenna. The geometry shows the top-side in black and the bottom-side in gray, where $r_{1a} = 22\,\text{mm}$, $r_{1b} = 39.6\,\text{mm}$, $r_2 = 9.8\,\text{mm}$, $t_1 = 0.2\,\text{mm}$, $t_2 = 0.4\,\text{mm}$, $l_r = 10\,\text{mm}$, $w_r = 24.5\,\text{mm}$, $l_{pa} = 15\,\text{mm}$ and $l_{pb} = 25\,\text{mm}$, $w_{50} = 0.93\,\text{mm}$, $l_f = 57.5\,\text{mm}$, $w_f = 0.5\,\text{mm}$, $l_g = 40\,\text{mm}$, and $B = 150\,\text{mm}$.

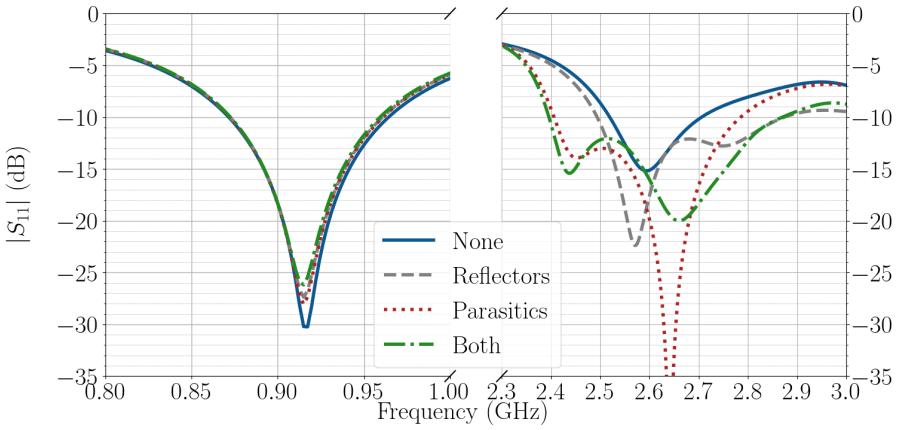

FIGURE 2. Simulated $|S_{11}|$ versus frequency in both the lower and upper bands for the antenna with various additional elements.

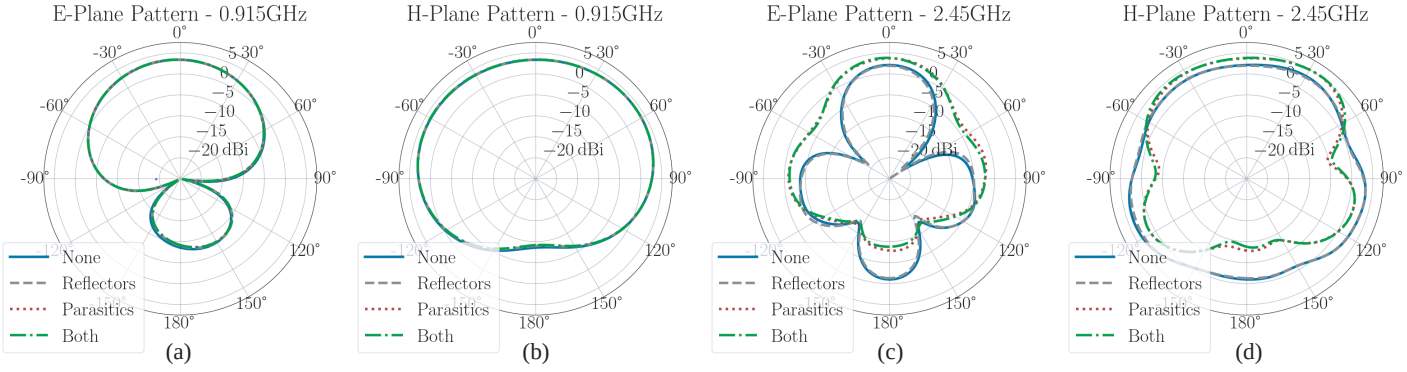

FIGURE 3. Simulated radiation patterns for (a) E-plane at 0.915 GHz, (b) H-plane at 0.915 GHz, (c) E-plane at 2.45 GHz, and (d) H-plane at 2.45 GHz for the antenna with various additional elements.

Figure 2 demonstrates that the effects of inserting these additional elements on the lower-band S_{11} characteristics are minimal. In contrast, the S_{11} performance at 2.45 GHz is dramatically improved by the addition of the parasitic elements. More specifically, the 10 dB return loss bandwidth improves from almost 7% to 19% by adding the parasitic and reflecting elements.

The antenna radiation patterns in each band are plotted in Fig. 3. There is very little difference in the lower-band radiation pattern from adding additional elements to the antenna. In con-

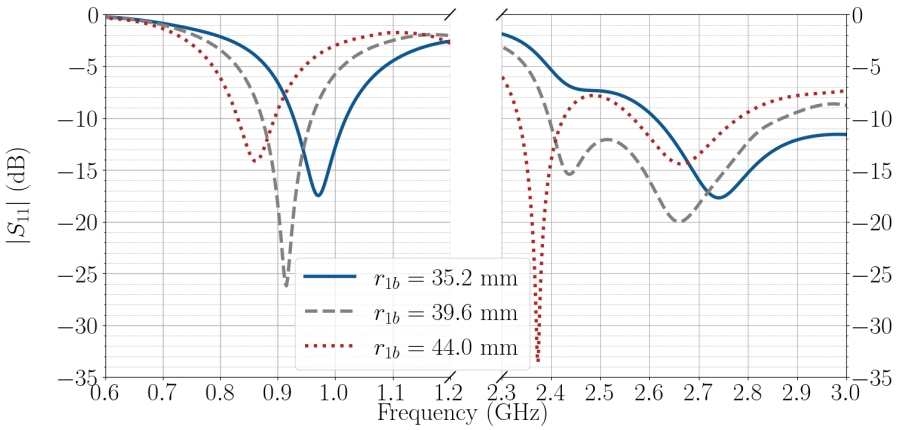

FIGURE 4. Simulated $|S_{11}|$ versus frequency in both the lower and upper bands for the antenna over a parametric sweep of the semi-major axis.

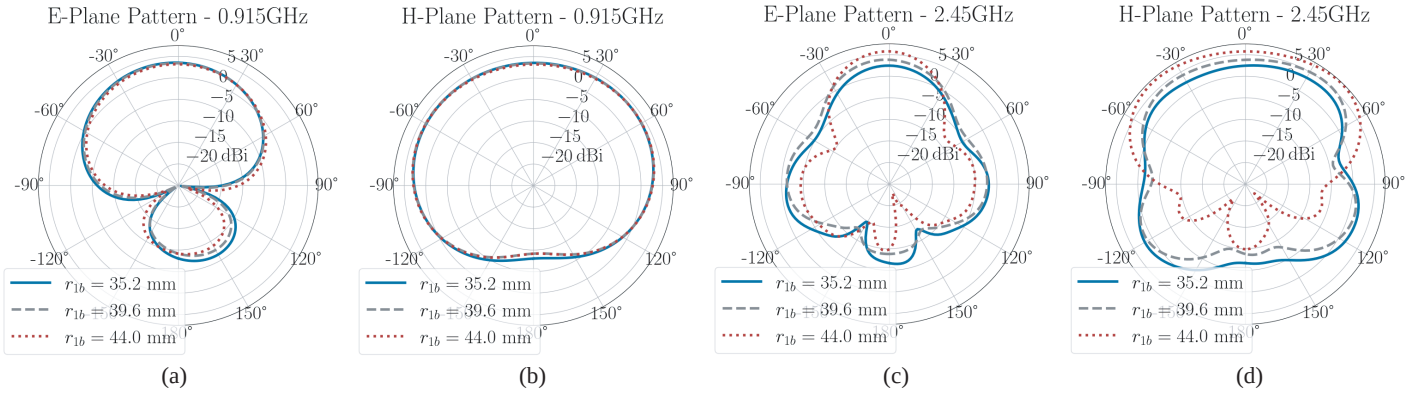

FIGURE 5. Simulated radiation patterns for (a) E-plane at 0.915 GHz, (b) H-plane at 0.915 GHz, (c) E-plane at 2.45 GHz, and (d) H-plane at 2.45 GHz over a parametric sweep of the semi-major axis.

trast, the parasitic elements provide significant improvement in the upper-band front-to-back ratio by attenuating the electromagnetic interactions between the lower- and upper-band arms, leading to about 2 dB and 8 dB improvement in the peak gain and front-to-back ratio, respectively.

3. PARAMETRIC SWEEP OF SEMI-MAJOR AXIS

A parametric sweep of the semi-major axis of the outer antenna arms was conducted to determine its effect on antenna performance. For the dual-band antenna shown in Fig. 1(a), the semi-major axis r_{1b} was initially chosen to be 39.6 mm. This sweep considered additional cases with semi-major axis values of 35.2 mm and 44.0 mm. For each of these cases, the semi-minor axis r_{1a} was held constant at 22 mm. As such, the eccentricity e could be calculated as

$$e = \sqrt{(1 - r_{1a}^2/r_{1b}^2)}. \tag{1}$$

As shown in Fig. 4, the resonant frequency in the lower band varied significantly with semi-major axis, being roughly dependent on the circumference of the outer ellipse. This explains the higher resonant frequency of 0.970 GHz for $r_{1b} = 35.2$ mm and a lower resonant frequency of 0.862 GHz for $r_{1b} = 44.0$ mm. Furthermore, the cases of both $r_{1b} = 35.2$ mm and $r_{1b} = 44.0$ mm resulted in return loss values well above the 10 dB level. The upper band return loss plot for both the $r_{1b} = 39.6$ mm and $r_{1b} = 44.0$ mm cases shows a dual-resonance behavior, with the first of these resonances placed near the target frequency of 2.45 GHz. For the $r_{1b} = 35.2$ mm case, however, this first resonance is significantly suppressed, and the 10 dB return loss band exists only at the higher end of that frequency range.

The gain patterns at both 0.915 GHz and 2.45 GHz are plotted in Fig. 5. Figs. 5(a) and 5(b) show little variance across the cases, so the radiation pattern in the lower band seems insensitive to changes in the eccentricity of the ellipse. In all cases, the peak gain is roughly 3.5 dBi, and the front-to-back ratio is within 0.5 dB of 12.1 dB. The radiation patterns in the upper band shown in Figs. 5(c) and 5(d) display more change across these cases. The peak gain at 2.45 GHz increases with the semi-major axis, with a difference of 3.3 dB at the extreme cases. The back lobe is also more greatly attenuated at higher eccentricities with a swing of more than 6.5 dB. These performance gains are significant and could warrant designing the antenna to have a higher eccentricity. It is also worth noting that the antenna efficiency is approximately 96.5% and 96.25% at the frequencies of 915 MHz and 2.45 GHz, respectively.

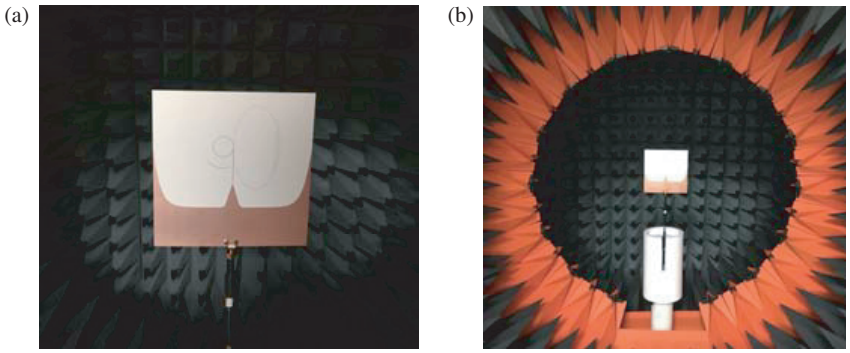

FIGURE 6. Proposed antenna prototype in UAH's spherical near-field anechoic chamber, (a) close-up photo of the antenna prototype, and (b) antenna under test.

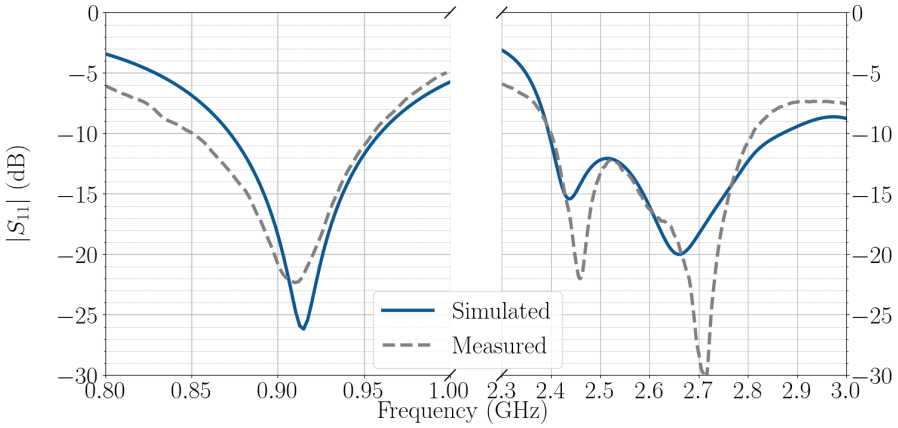

FIGURE 7. Simulated and measured $|S_{11}|$ of the antenna prototype versus frequency for both the lower and upper bands.

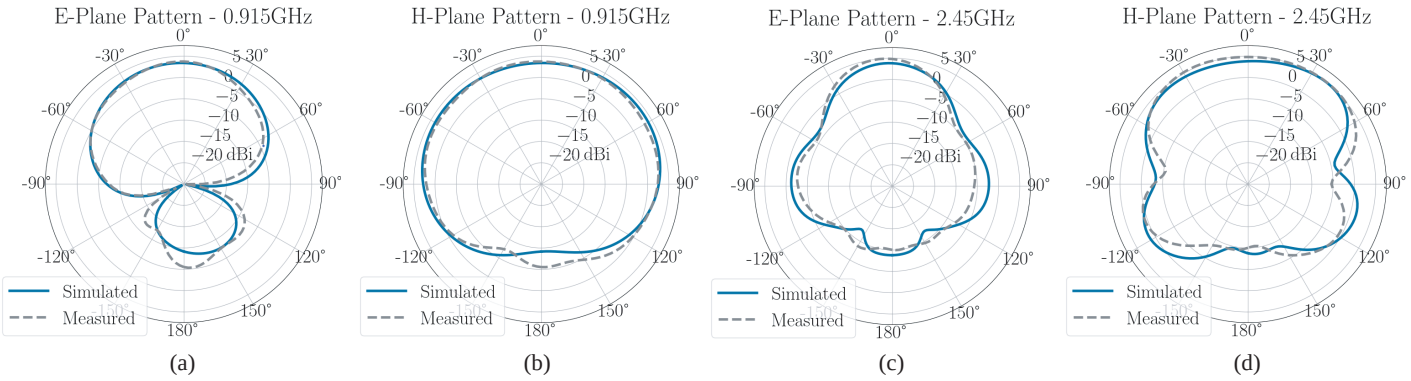

FIGURE 8. Simulated and measured radiation patterns for (a) E-plane at 0.915 GHz, (b) H-plane at 0.915 GHz, (c) E-plane at 2.45 GHz, and (d) H-plane at 2.45 GHz.

4. MEASURED RESULTS

The dual-band outline elliptical outline design in Fig. 1(a) was then fabricated and measured with a vector network analyzer and the spherical near-field anechoic chamber of the University of Alabama in Huntsville (UAH). The manufactured antenna under test is displayed in UAH's anechoic chamber in Fig. 6.

Figure 7 shows the S_{11} performance across each of the bands of interest, exhibiting good agreement between the measured and simulated results. We can see that in the lower band, the antenna has a return loss of 26.2 dB at 0.915 GHz in simulation compared with the experimentally measured 21.87 dB. The simulated resonant frequency in the lower band is 0.915 GHz, while the measured resonant frequency is 0.910 GHz. The 10 dB return loss bandwidth is simulated as 85 MHz or 9.30% and measured as 103 MHz or 11.26%. The upper-band portion of Fig. 7 shows that there are two different resonant frequencies which contribute to the wideband nature of the upper band. The first of these resonances is close to the design fre-

TABLE 1. Comparison between the proposed dual-band antenna and other state-of-the-art antenna designs.

Dual-Band Antenna Design	Area in lowest band (λ^2)	Lower-band Measured Gain (dBi)	Upper-band Measured Gain (dBi)
Double-T Monopole Antenna [14]	0.360	1.8	1.5
Frame-printed dipole Antenna [16]	0.230	1.77	2.17
Dual-band printed Antenna [18]	0.246	1.48	3.83
Reconfigurable Bowtie Antenna [19]	0.144	0.02	2.80
This work	**0.209**	**3.75**	**4.81**

quency; in simulation, it is 2.44 GHz, and in measurement it is 2.46 GHz. The second of these resonances, 2.66 GHz in simulation and 2.71 GHz in the measured data, is closer to three times of the lower-band design frequency. The simulated and measured 10 dB return loss bandwidths are approximately 19% and 15.5%, respectively.

The antenna radiation patterns were also measured in UAH's near-field anechoic chamber at both 0.915 GHz and 2.45 GHz. These patterns for the E-plane and H-plane cuts are compared to the simulated results in Fig. 8, exhibiting good agreement at both bands. Figs. 8(a) and 8(b) show a more pronounced back lobe for the measured antenna in the lower band, which is in part attributed to the reflections caused by the connecting cable in the anechoic chamber.

Figures 7 and 8 show that overall measurements of the prototype follow closely with their simulated counterparts. The 10 dB return loss bandwidths, though different from the simulation, are still acceptable. Similarly, the measured front-to-back ratio at 0.915 GHz is close to the desired 10 dB, and some degradation is expected due to the mounting setup in the anechoic chamber. Finally, the measured peak gain is close to the simulated value, within 1 dB, which is well within the gain error of the antenna test range.

5. CONCLUSION

A novel dual-band elliptical antenna design is presented in this article. The two pairs of outline antenna arms, exponentially tapered ground plane, reflectors behind the upper-band elements, and parasitic strips within the lower-band arms all contribute to an antenna that works well at both 0.915 GHz and 2.45 GHz. This proposed antenna achieved greater than 14 dB return loss, 3.4 dBi peak gain, and 12 dB front-to-back ratio. It is compact and has good measured peak gain in each band compared to other designs as Table 1 suggests. The antenna used for comparison with [14] was their antenna 4. As for radiation characteristics, the novel outline elliptical antenna presented here is unidirectional whereas the antennas shown in [14, 16, 18, 19] are bidirectional, suggesting that the proposed design is preferable whenever such a radiation pattern is desired within a smaller physical area. As such, this new antenna is a promising candidate for space-based passive energy harvesting applications.

ACKNOWLEDGEMENT

The authors would like to thank Jonathan Shreve for his help in re-plotting the scattering parameters and radiation patterns in Python.

REFERENCES

[1] Arrawatia, M., M. S. Baghini, and G. Kumar, "Broadband bent triangular omnidirectional antenna for RF energy harvesting," *IEEE Antennas and Wireless Propagation Letters*, Vol. 15, 36–39, 2015.

[2] Duffley, B. G., G. A. Morin, M. Mikavica, and Y. M. M. Antar, "A wide-band printed double-sided dipole array," *IEEE Transactions on Antennas and Propagation*, Vol. 52, No. 2, 628–631, Feb. 2004.

[3] Tu, Z., G.-Q. Zhang, D.-F. Zhou, and F. Xing, "A wideband elliptic printed dipole antenna array," in *2011 4th IEEE International Symposium on Microwave, Antenna, Propagation and EMC Technologies for Wireless Communications*, 68–70, Beijing, China, Nov. 2011.

[4] Durgun, A. C., C. A. Balanis, C. R. Birtcher, and D. R. Allee, "Design, simulation, fabrication and testing of flexible bow-tie antennas," *IEEE Transactions on Antennas and Propagation*, Vol. 59, No. 12, 4425–4435, Dec. 2011.

[5] Nakano, H., S. Hattori, H. Mimaki, and J. Yamauchi, "A card-type wide band antenna," *IEICE Proceedings Series*, Vol. 33, No. 3A3-3, Nov. 2005.

[6] Azenui, N. C. and H. Y. D. Yang, "A printed crescent patch antenna for ultrawideband applications," *IEEE Antennas and Wireless Propagation Letters*, Vol. 6, 113–116, 2007.

[7] Abbosh, A. M. and M. E. Bialkowski, "Design of ultrawideband planar monopole antennas of circular and elliptical shape," *IEEE Transactions on Antennas and Propagation*, Vol. 56, No. 1, 17–23, Jan. 2008.

[8] Werner, D. H., "Exact expressions for the far-zone electromagnetic fields radiated by thin elliptical loop antennas of arbitrary size," *IEEE Transactions on Antennas and Propagation*, Vol. 66, No. 12, 6844–6850, Dec. 2018.

[9] Nazli, H., E. Bicak, B. Turetken, and M. Sezgin, "An improved design of planar elliptical dipole antenna for UWB applications," *IEEE Antennas and Wireless Propagation Letters*, Vol. 9, 264–267, 2010.

[10] Tziris, E. N., P. I. Lazaridis, Z. D. Zaharis, J. P. Cosmas, K. K. Mistry, and I. A. Glover, "Optimized planar elliptical dipole antenna for UWB EMC applications," *IEEE Transactions on Electromagnetic Compatibility*, Vol. 61, No. 4, 1377–1384, Aug. 2019.

[11] De Noia, V., A. Alves, M. Diaz, and R. Barroso, "Input impedance behavior of a planar elliptical ring dipole antenna,"

in *Proceedings of the 2012 IEEE International Symposium on Antennas and Propagation*, 1–2, Chicago, IL, USA, Jul. 2012.

[12] Maci, S., G. B. Gentili, P. Piazzesi, and C. Salvador, "Dual-band slot-loaded patch antenna," *IEE Proceedings-Microwaves, Antennas and Propagation*, Vol. 142, No. 3, 225–232, Jun. 1995.

[13] Kim, S. M. and W. G. Yang, "Design and implementation of dual wideband sleeve dipole type antenna for the reception of S-DMB and 2.4/5 GHz WLAN signals," in *2006 IEEE Antennas and Propagation Society International Symposium*, 981–984, Albuquerque, NM, Jul. 2006.

[14] Kuo, Y.-L. and K.-L. Wong, "Printed double-T monopole antenna for 2.4/5.2 GHz dual-band WLAN operations," *IEEE Transactions on Antennas and Propagation*, Vol. 51, No. 9, 2187–2192, Sep. 2003.

[15] Joshi, R. K. and A. R. Harish, "A modified bow-tie antenna for dual band applications," *IEEE Antennas and Wireless Propagation Letters*, Vol. 6, 468–471, 2007.

[16] Wu, P., Z. Kuai, and X. Zhu, "Multiband antennas comprising multiple frame-printed dipoles," *IEEE Transactions on Antennas and Propagation*, Vol. 57, No. 10, 3313–3316, Oct. 2009.

[17] Song, C. T. P., P. S. Hall, and H. Ghafouri-Shiraz, "Multiband multiple ring monopole antennas," *IEEE Transactions on Antennas and Propagation*, Vol. 51, No. 4, 722–729, Apr. 2003.

[18] Bhatt, K., S. Kumar, P. Kumar, and C. C. Tripathi, "Highly efficient 2.4 and 5.8 GHz dual-band rectenna for energy harvesting applications," *IEEE Antennas and Wireless Propagation Letters*, Vol. 18, No. 12, 2637–2641, Dec. 2019.

[19] Li, T., H. Zhai, X. Wang, L. Li, and C. Liang, "Frequency-reconfigurable bow-tie antenna for Bluetooth, WiMAX, and WLAN applications," *IEEE Antennas and Wireless Propagation Letters*, Vol. 14, 171–174, 2014.